Comparison of the Effects of k-ϵ, k-ω, and Zero Equation Models on Characterization of Turbulent Permeability of Porous Media

Charlie Matsubara*, Tim Kuo, Helen Wu

PIM Consulting, No. 16, Gonyequ 1st Road, Taichung City, Taiwan

*pimconsultinginc@gmail.com

***Abstract*- In this study, different turbulent models were used ($k-\varepsilon, k-\omega,$ and zero equation models) to characterize the permeability of turbulent water flows (hydraulic conductivity) in an artificial crack. The results were compared to a "universal" equation of flow in porous media based on empirical fit (Barr's model) of a simple general check. The results showed that while the simulations did not match the empirical model, they follow the same trends. The values of the empirical constants in Barr's model can be modified to match that of the simulation results. The results then were compared against the simulation results and were found to be mildly sensitive to the type of turbulent model used. In this problem, $k-\omega$ was considered to be most suitable model, due to limitations of the other models. The discrepancies between the $k-\epsilon$, $k-\omega$ and zero equation models were small, less than 5%. These discrepancies may be due to the nature of the scenario of interest and simplifications that were applied to it.**

***Keywords*- Turbulent Models; Darcy's Law; Hydraulic Conductivity; Porous Media; CFD**

I. INTRODUCTION

Personal computers have reached the stage where they can be used to conduct quality research work as research commercial software becoming more increasingly mature to be used to help solve complex problems. One of such a problem is turbulent flows in porous media. Porous media evaluation is important for the development of oil and gas reservoirs. In the fields of hydraulic fracturing and enhanced oil recovery, understanding turbulent flows in porous media is important to control and improve petroleum extraction. To date, most of the modelling efforts in the field of turbulent flows in porous media have been heavily reliant on empirical fits of the few data available. By performing computational fluid dynamics (CFD) simulations of flow of different fluid mixtures through these generated porous media, using either a Navier-Stokes solver or the Lattice Boltzman method [1-2], macroscopic transport properties such as permeability and relative permeability can be predicted. Currently, the scale of CFD simulations is limited at larger scales due to limitations in computational resources and the complexity of porous media.

Currently, there are existing mature codes to simulate flow in porous media such as TOUGH2. However, these mature codes rely on Darcy's law, which is based on Fourier's law. Darcy's law only applies for slow laminar flow, thus, turbulent phenomena that would affect transport flow are not captured [3]. Conducting major modifications of existing mature codes would not be desirable as solving the nonlinear terms would be expensive at large scales. Turbulent flows in porous media can be found in injection and leakage sites. In this paper, an investigation of modification of existing parameters in Darcy's law to help capture the turbulent flow is proposed.

Darcy's law states that the Darcy discharge (discharge rate, Q) through a porous medium, is proportional to the hydraulic gradient (dh/dx), permeability (k), and cross-sectional area (A) of the media and inversely proportional to the viscosity of the fluid (μ), which results in hydraulic conductivity (K) if fluid is water, shown in Equation (1). Hydraulic conductivity is the ability for a porous media to transmit water, which is closely related to permeability. Hydraulic gradient is defined as a change of hydraulic head over distance. Hydraulic head is composed of pressure head, elevation head, and velocity head, which means energy per unit weight, this is equivalent to the total pressure head [3]. Usually, velocity head is neglected as the magnitude of the velocity head is much smaller than the other components; however, velocity head cannot be neglected in this study due to the high velocity nature of the problem [4].

The permeability of a porous medium has been defined as an intrinsic material property and is determined experimentally or numerically. While this simple relation is applied in major porous media flow simulators, it is only valid in low Reynolds number and ultimately breaks down at higher Reynolds numbers [5]. The inaccuracy due to the limitation is shown in Fig. 1.

$$Q = -\frac{kA}{\mu}\left(\frac{dh}{dx}\right) = K\left(-\frac{dh}{dx}\right) \tag{1}$$

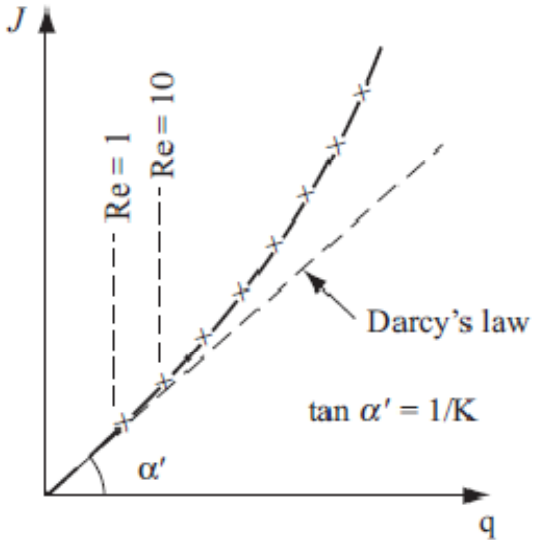

Fig. 1 Experimental relationship between specific discharge, q, and hydraulic gradient, J, of sand under different Reynolds numbers (Bear and Cheng, 2010)

In this paper, an artificially created crack commonly found in porous media was created to simulation flow through a crack in scenarios found in leakage and injection sites. Different turbulent models, k-ε, k-ω, and zero equation models, were used in this project to determine the effects of different turbulent schemes and evaluate against the empirical model developed by Barr [6].

II. BARR'S MODEL

Numerous modifications and extensions to Darcy's law have been proposed [7]. These extensions and modifications almost always include extra nonlinear terms that require major overhaul of the existing codes. The motivation of this work is to determine the equivalent hydraulic conductivity found in Darcy's law for turbulent flow for use of the existing solvers.

The idea of equivalent turbulent hydraulic conductivity was investigated by Barr [8]; however, his derivation of an universal conductivity for both laminar and turbulent flow is based on parameters that are not easily measured for naturally occurring porous media. Barr derived this model based on duct flow with modifications to capture turbulence phenomenon and then "tweaked" the numerical coefficients seen in Equation (2) and Equation (4) against experimental data. The work was not evaluated against carefully controlled experiments or simulations. Much of the experimental data compared with had missing information on important parameters as well as large experimental errors. Nevertheless, in the poorly understood field of hydrogeology, the model developed by Barr can prove to be a general check.

His model followed Darcy's law with modifications of hydraulic conductivity, called *Ke*, seen in Equation 1, where *K* is the laminar hydraulic conductivity, ϕ is the porosity, *V* is the Darcy discharge, R_h is the hydraulic radius. Subbing Equation (2) into Darcy's law, which resulted in the general form of flow in porous media as derived, seen in Equation (3). In most practical applications, either the discharge or the head gradient will be known.

$$K_e = \left(\frac{1}{K} + \frac{\sqrt{2}V}{3\phi^2 g R_h} \right)^{-1} \tag{2}$$

$$\frac{V}{K\left(-\frac{dh}{dx}\right)} + \frac{\sqrt{2}V^2}{3\phi^2 g R_h\left(-\frac{dh}{dx}\right)} - 1 = 0 \tag{3}$$

$$K = \rho g \phi \frac{R_h^2}{5\mu} \tag{4}$$

III. TURBULENCE MODELS

Three ANSYS turbulence models were used for these simulations.

A. Zero Equation Model

This is a simple eddy viscosity model to compute a value for $\mu_t = \rho f_\mu U_t l_t$ from the mean velocity and length scales ($l_t = \frac{V_D^{\frac{1}{3}}}{7}$) using an empirical formula. There are no additional transport equations to be solved, thus this is called zero equation model [9].

B. k-ε Model

The turbulence kinetic energy is defined as the variance of the fluctuations in velocity. The turbulence eddy dissipation is the rate at which the velocity fluctuations dissipate. The values of k and ε come from transport equations for turbulent kinetic energy and turbulent dissipation rate shown in Equations (5) and (6) [9].

$$\frac{\partial(\rho k)}{\partial t} + \nabla.(\rho U k) = \nabla.\left(\left(\mu + \frac{\mu t}{\sigma k}\right) + \nabla k\right) + P_K + P_{Kb}\varepsilon - \rho\varepsilon \tag{5}$$

$$\frac{\partial(\rho\varepsilon)}{\partial t} + \nabla\cdot(\rho U\varepsilon) = \nabla\cdot\left(\left(\mu + \frac{\mu_t}{\sigma_\varepsilon}\right) + \nabla\varepsilon\right) + \frac{\varepsilon}{k}(C_{\varepsilon 1}(P_k + P_{\varepsilon k}) - C_{\varepsilon 2}\rho\varepsilon) \tag{6}$$

P_{kb} and $P_{\varepsilon b}$ represent the influence of buoyancy forces. P_K is the turbulence production due to viscous forces. $C_{\varepsilon 1}$, $C_{\varepsilon 2}$, σ_k, and σ_ε are constants and are valued as 1.44, 1.92, 1, and 1.3, respectively [9].

C. k-ω Model

One of the advantages of k-ω model is the near wall treatment. The model is more accurate and robust. The model assumes that the turbulent viscosity is linked to the turbulent kinetic energy and the turbulent frequency. It solves two equations, one for turbulent kinetic energy and the other for turbulent frequency shown in Equations (7) and (8) [9].

$$\frac{\partial(\rho k)}{\partial t} + \nabla\cdot(\rho U k) = \nabla\cdot\left(\left(\mu + \frac{\mu_t}{\sigma_k}\right) + \nabla k\right) + P_k + P_{kb} - \beta'\rho k\omega \tag{7}$$

$$\frac{\partial(\rho\omega)}{\partial t} + \nabla\cdot(\rho U\omega) = \nabla\cdot\left(\left(\mu + \frac{\mu_t}{\sigma_\omega}\right) + \nabla\omega\right) + \alpha\frac{\omega}{k}P_k + P_{\omega b} - \beta\rho\omega^2 \tag{8}$$

P_{kb} and $P_{\omega b}$ represent the influence of buoyancy forces. P_k is the turbulence production due to viscous forces. α, β, β', σ_k, and σ_ω are constants and are valued as 5/9, 0.075, 0.09, 2, and 2 respectively [9].

IV. RESULTS

A long and irregular crack was drawn in ANSYS, for simplicity, the only a slither of the crack was modelled for simplicity and symmetry boundary conditions were applied at the sides, treating it as a two-dimensional crack. The physical properties of the crack are shown in Table 1. The inlet has a width of 4.18 cm while outlet has a width of 7.34 cm. The inlet area in the model has area of 0.00487 m^2 and outlet area of 0.00734 m^3, while the length of the crack is 52.9 cm. The hydraulic radius was calculated by the volume of the crack divided by the total surface area. The Reynolds numbers were found using the hydraulic diameter, in the range of 104 to 106. The fluid simulated was water at 25^0C and pressure of 1 atm, with density of 997 kg/m3 and dynamic viscosity of $8.9x10^{-4}$ PaS. The convergence criterion was set to be 10^{-4}.

TABLE I PHYSICAL PROPERTIES OF THE CRACK

Surface Area of Inlet (m^2)	Surface Area of Outlet (m^2)	Total Surface Area (m^2)	Volume (m^3)	Hydraulic Radius (m)	Porosity	Hydraulic Conductivity (m/s)
4.87E-03	7.34E-03	1.11E-01	0.003117	2.81E-02	1.00E+00	1.73E+03

Constant velocities of 0.5 m/s, 1 m/s, 5 m/s, 8 m/s, and 10 m/s were applied at the inlet with turbulence intensity of 5%, while outlet maintained static pressure of 0 atm. Two mesh sizes were applied for this problem, coarse and fine. For the fine mesh, inlet velocity of 8 m/s was neglected as it did not provide extra information. The boundary conditions were set so that conservation of mass can be easily applied in the longitudinal direction to find the exact theoretical velocity in the x-direction. The numerical experiments conducted were performed in Reynolds numbers in the range of 104 and 106, since it is unlikely to find fluid flowing faster than that in geological formations without causing change in geological formations.

The walls were considered to be smooth with no-slip conditions, to simplify the problem. No attempts were made to calculate the pressures at the inlet and outlet by Bernoulli equation as losses due to forces, such as external forces and shear forces, are neglected. Any analytical results would have to be based on velocity head from conservation of mass applied in the longitudinal direction. This is a good check for the results of the simulations as velocity (x-direction) head should be the dominant in this study. The geometry and boundary conditions applied are shown in Fig. 2.

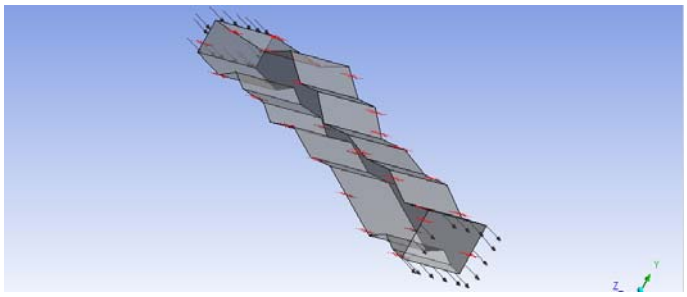

Fig. 2 A long and irregular crack with symmetric boundary conditions on the sides

The mesh type selected was quadrilateral mesh with two difference sizes. The coarse mesh size had maximum size constraint of 0.0075 m while the fine mesh size had constraint of 0.005 m. These two meshes are seen in Fig. 3 and Fig. 4.

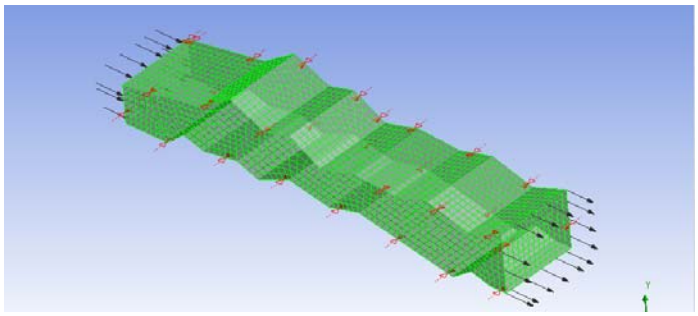

Fig. 3 Coarse mesh of 0.0075m

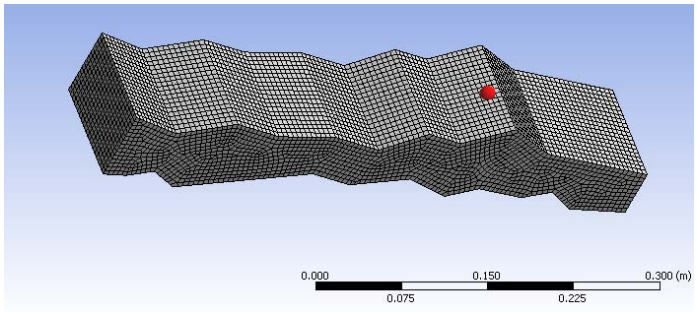

Fig. 4 Fine mesh of 0.005m

The results from turbulent models were graphed along side with Barr's model and hand calculations based on longitudinal velocity head can give any idea of the general trend. These results are seen in Table 2, and Table 3. Fig. 5 shows the hydraulic gradients with varying velocities for all three turbulent models, the calculated velocity along x-direction, and Barr's model (experimental). Table 3 shows the deviations of the Darcy velocities and hydraulic conductivities between different turbulent models where Barr's model and zero equation were used as benchmarks. It was found by refining the mesh, the results changed by less than 9%, meaning the solutions have converged by engineering standard. Fig. 6 shows the hydraulic conductivity profiles with Reynolds numbers.

TABLE II FINE MESH RESULTS

Method	Inlet Velocity (m/s)	Outlet Average Velocity (m/s)	Hydraulic Gradient (m/m)	Velocity Head Gradient (m/m)	Outlet Reynolds Number
0 Equation	0.5	3.37E-01	-1.91E-02	-1.32E-02	1.35E+04
0 Equation	1	6.74E-01	-7.41E-02	-5.26E-02	2.71E+04
0 Equation	5	3.37E+00	-1.77E+00	-1.32E+00	1.35E+05
0 Equation	10	6.74E+00	-7.00E+00	-5.26E+00	2.71E+05
$k-\varepsilon$	0.5	3.38E-01	-1.87E-02	-1.31E-02	1.36E+04
$k-\varepsilon$	1	6.77E-01	-7.31E-02	-5.22E-02	2.72E+04
$k-\varepsilon$	5	3.39E+00	-1.77E+00	-1.30E+00	1.36E+05

k – ε	10	6.79E+00	-7.00E+00	-5.21E+00	2.72E+05
k – ω	0.5	3.37E-01	-1.71E-02	-1.32E-02	1.35E+04
k – ω	1	6.73E-01	-6.65E-02	-5.28E-02	2.70E+04
k – ω	5	3.36E+00	-1.61E+00	-1.32E+00	1.35E+05
k – ω	10	6.72E+00	-6.39E+00	-5.28E+00	2.70E+05

TABLE III VELOCITY/HYDRAULIC CONDUCTIVITY DEVIATIONS (%) IN DIFFERENT TYPES OF MESH AND TURBULENCE MODELS

Mesh Type	Turbulence Model	Velocity/Hydraulic Conductivity Deviations from Barr (%)	Velocity/Hydraulic Conductivity Deviations from 0 Equation Model (%)
Coarse Mesh	0 Equation	67.67	N/A
	k-epsilon	66.86	0.33
	k-omega	66.56	3.32
Fine Mesh	0 Equation	66.90	N/A
	k-epsilon	66.59	0.45
	k-omega	65.26	4.94

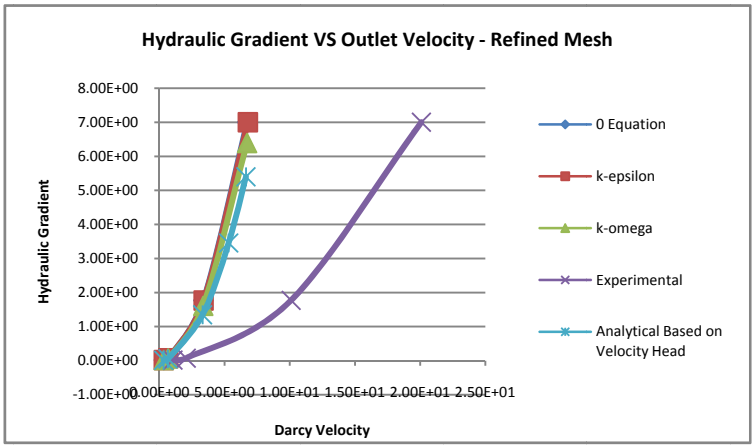

Fig. 5 Hydraulic gradient VS outlet velocity in fine mesh

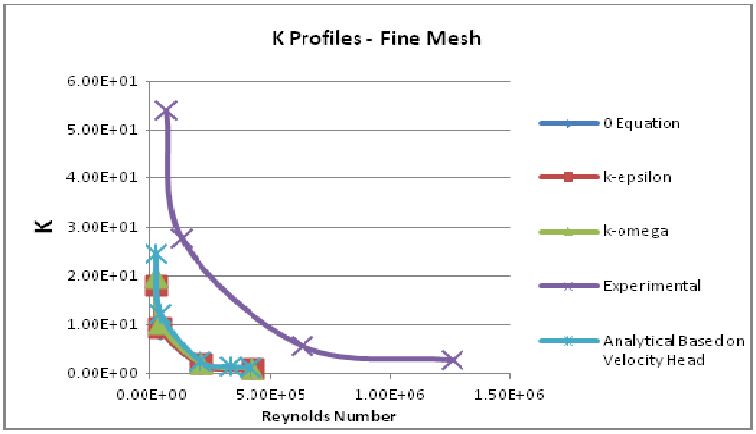

Fig. 6 Hydraulic conductivity profiles in different Reynolds Numbers

Comparing the results from the turbulent models used along side with Barr's model and calculations based on velocity head (Bernoulli equation) can give any idea of the general trend. All three turbulent models yielded very similar results. From Table 3, the results from zero equation were used as benchmark to see how much the Darcy velocities and hydraulic conductivities differ between different turbulent models, which showed that the other two turbulent models are within 5% of each other. The simulation results deviated quite from far Barr's results seen in Table 3; however, results from Barr's model were meant to be used as a "right order of magnitude" check. These results also show that while the velocity head in the longitudinal direction is dominant, the transverse velocity heads and pressure heads play important roles.

Fig. 6 shows the hydraulic conductivity profiles with Reynolds numbers. They also show similar trends as Barr's model. While Barr's results and the simulation results are different but the general profile is identical, this is a good indication that the simulations results are in the right ballpark. In fact, Barr's model constants could be tweaked to give exact results as the simulations. The profile based on longitudinal velocity head showed that the simulations are in line with what were expected.

Further work was done to show that refining of the mesh did little to change the result; therefore, it is safe to say that the space discretization errors are small and the solution had converged by engineering standards. While the results so far showed that in terms of fluid migration at injection or leakage sites, all three turbulent models can produce adequate results, it is still important to analyse the phenomena that caused the slight differences in each. This can be seen in the velocity vector plots in Fig. 7, Fig. 8, and Fig. 9.

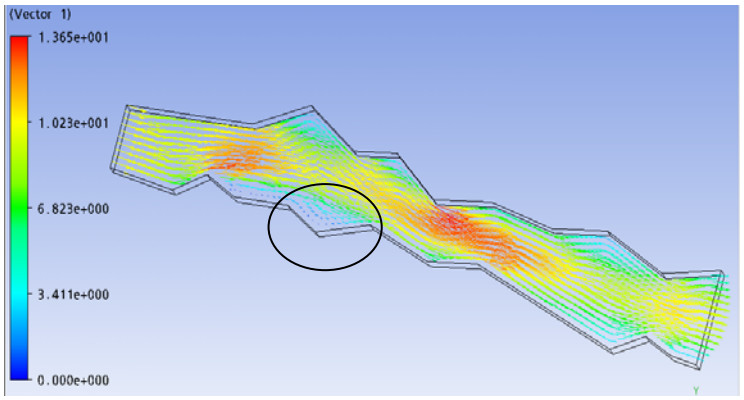

Fig. 7 Zero equation vector velocity plot at inlet velocity of 10 m/s

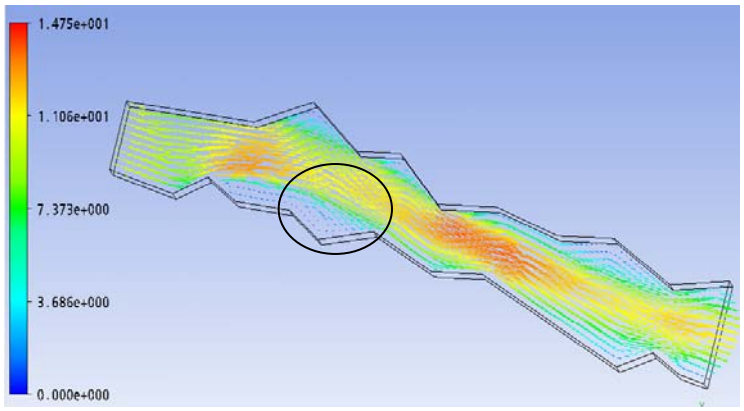

Fig. 8 $\mathbf{k-\varepsilon}$ model vector velocity plot at inlet velocity of 10m/s

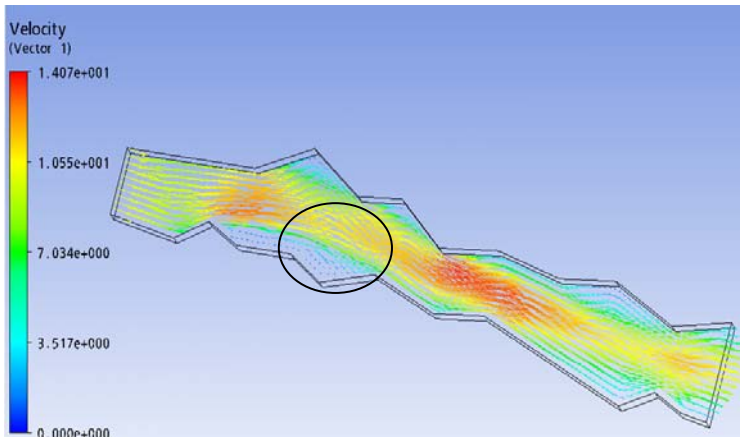

Fig. 9 $\mathbf{k-\omega}$ model vector velocity plot at inlet velocity of 10m/s

One of the limitations of the zero equation model is the lack of ability to capture recirculation and flow around obstacles (Devaud, 2011; Pope, 2000). This is evident in the vector velocity field of the zero equation model show in Fig. 7. This could explain the 3-5% difference when compared with results from the $k-\omega$ model as $k-\omega$ model has the best wall treatment of the three models. While zero equation model has its limitations, it was significantly faster than the other two models. A simulation at fine mesh could be done in a fraction of the time it took to run the other simulations on a PC. This is an advantage when quick results are desired.

Fig. 8 and Fig. 9 show the velocity vector plots for k – ω model and k – ε model. It is difficult to spot any differences between the two other than the different maximum velocity. Both models captured the recirculation behind obstacles. The k – ε model predicts well in plane jets and flat boundary conditions, while performs poorly in far wake obstacles and sudden contractions (Devaud, 2011; Pope, 2000). The k – ω model is superior in its treatment of viscous layer near wall regions while treatment of non-turbulent free stream boundaries is problematic (Devaud, 2011; Pope, 2000). While these differences are hard to capture in vector velocity plots, they can be seen in the turbulent kinetic energy profiles.

Fig. 10 and Fig. 11 show some differences in turbulent kinetic energies between the two two-equation models. It was noticed that k – ε results showed higher turbulent kinetic energy than k – ω results at the regions marked by circles. The regions marked by rectangles show that k – ω model predicted higher turbulent kinetic energy than k – ε results.

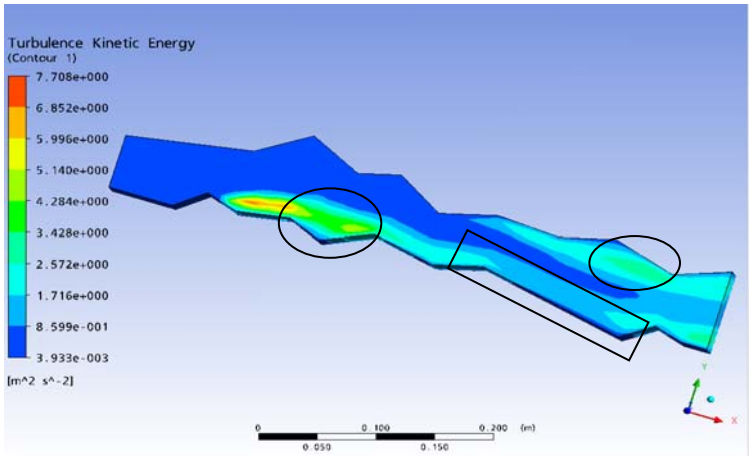

Fig. 10 **k – ε** model turbulent kinetic energy plot at inlet velocity of 10m/s

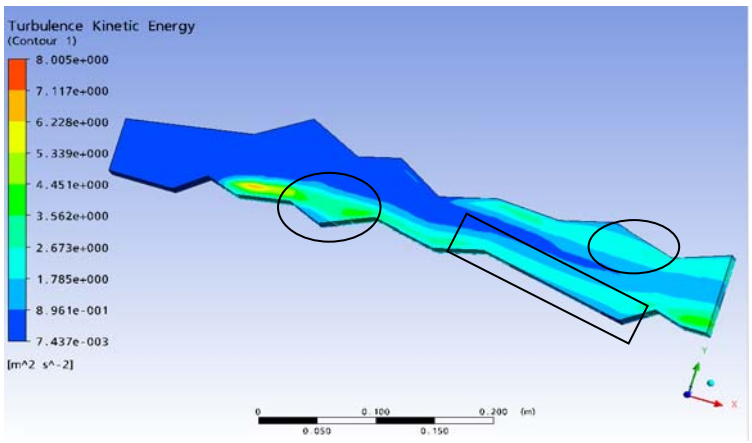

Fig. 11 **k – ω** model turbulent kinetic energy plot at inlet velocity of 10m/s

From Fig. 12 and Fig. 13, it is easy to spot the differences in the turbulent eddy dissipation predicted by the two two-equation models. These differences are most apparent at sudden contraction and in the wake region, where k – ε model performs poorly.

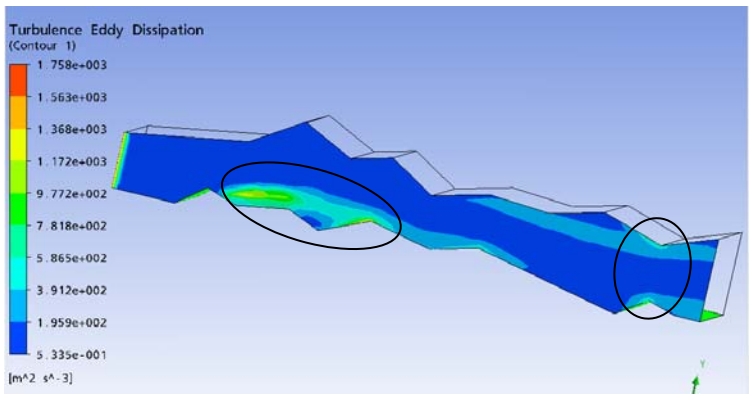

Fig. 12 **k – ε** model turbulent eddy dissipation plot at inlet velocity of 10m/s

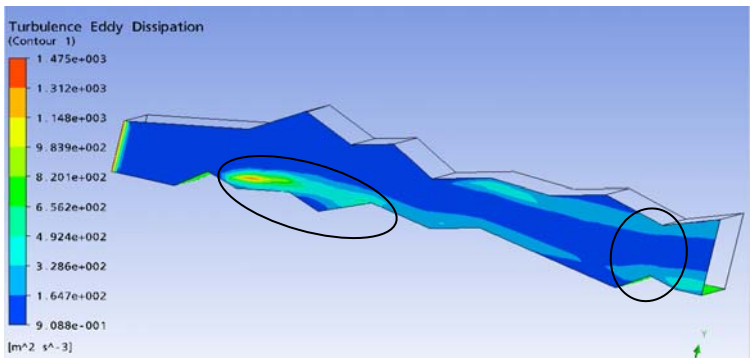

Fig. 13 $\mathbf{k-\omega}$ model turbulent eddy dissipation plot at inlet velocity of 10 m/s

Comparing these differences and relating back to the limitations of each model, it would seem like the $k-\omega$ model is more suitable for this problem. Perhaps larger discrepancies between models would be apparent if roughness of the walls and inclusion of dead pores in the porous media were taken into account. Previous work by Kuznetsov [10] has also shown that surface roughness significantly impacts the turbulent flow.

V. CONCLUSIONS

This paper evaluated the different turbulent models used in ANSYS, $k-\epsilon$, $k-\omega$, and zero equation models, to characterize the hydraulic conductivity of turbulent water flow in an artificial crack. These results were compared with Barr's model and the calculation based on conservation of mass as checks.

The results showed that Barr's model and the simulated results have similar trends and the simulation results were in the right order of magnitude. Barr's model served as a general check and the empirical constants in the model could also be adjusted to match the simulation results. The calculation based on conservation of mass showed that while longitudinal velocity component is dominant, other components of the hydraulic head still play important roles.

The differences between the turbulent models were found to be small, less than 5%, despite of the fundamental differences in the nature of the turbulence models. This perhaps was due to the nature of the scenario of interest and simplifications that were applied to it. Nevertheless, based on the limitations and strength of the evaluated models, $k-\omega$ was considered to be most suitable model for the scenario.

The discrepancy between models, however small, is probably due to the limitations of each model. This was seen in velocity field comparisons, where the zero equation model did not capture flow recirculation. Differences in results from $k-\epsilon$ and $k-\omega$ models were made clear from turbulent eddy dissipation and turbulent kinetic energy analysis. These differences are caused by the inability of $k-\epsilon$ model in situations of sudden contractions and far wake behind obstacles. For this scenario, it was found that the values of permeability/hydraulic conductivity are largely insensitive to the turbulent model used.

The results of this study are relevant to the field of hydraulic fracturing and enhanced oil recovery. Future works from this project will include complex geometries, surface roughness, and multiphase flows.

ACKNOWLEDGMENT

Here, we would like to give thanks to Mr. Jim Kuo from PIM Consulting for his invaluable advice and continuous support.

REFERENCES

[1] S. Chen, G.D. Doolen, *Lattice Boltzmann Method for Fluid Flows*, Annu. Rev. Fluid Mech., vol. 30, pp. 329-364, 1998.

[2] B. Ferreol, D.H. Rothman, *Lattice Boltzmann simulations of flow through Fontainebleau sandstone*, Trans. Porous Media, vol. 2, pp. 3-20, 1995.

[3] G. Brown, *Henry Darcy and His Law*, in, 2006.

[4] J. Bear, A.H.-D. Cheng, *Modeling Groundwater Flow and Contaminant Transport*, *1st ed*., Springer, 2010.

[5] W.E.S.a.C.E.N. Steven E. Ingebritsen, *Groundwater in Geologic Processes*, *Second Edition ed*., Cambridge University Press, 2006.

[6] D.W. Barr, *Coefficient of Permeability Determined By Measurable Parameters*, Ground Water, vol. 39, pp. 356-361, 2000.

[7] D.L.K. A. Firoozabadi, *An analysis of high-velocity gas flow through porous media*, Journal of Petroleum Technology, vol. 31, pp. 211-216, 1979.

[8] D.W. Barr, *Turbulent Flow Through Porous Media*, Ground Water, vol. 39, pp. 646-650, 2001.

[9] I. ANSYS, *ANSYS CFX-Solver Theory Guide*, in, Canonsburg, pp. 56-59, 2009.

[10] A.V. Kuznetsov, *Numerical modelling of turbulent flow in a composite porous/fluid duct utilizing a two-layer $k-\epsilon$ model to account for interface roughness*, International Journal of Thermal Sciences, vol. 43, issue 11, pp. 1047-1056, 2004.